Asian Journal of Chemistry; Vol. 38, No. 8 (2026), 2025-2036
ASIAN JOURNAL OF CHEMISTRY
https://doi.org/10.14233/ajchem.2026.36184

Thermally Activated Construction Waste-Derived Silicate Adsorbents for Benzene Removal in Aqueous Solution Using Fixed-Bed Column Studies

SENTHIL KUMAR MUNIASAMY[1,*], GOPALA KRISHNA GUMPALLI VENKATA THIRUMALA[2], M. MANIMARABOOPATHY[3], V. VELMURUGAN[3] and A. SIVAKAMI[4,*]

[1]Department of Biotechnology, Karpaga Vinayaga College of Engineering and Technology, Karpaga Vinayaga Educational Lore for Learning (Deemed to be University), Chinna Kolambakkam, Chengalpattu-603308, India
[2]Department of Civil Engineering, PSNA College of Engineering and Technology, Kothandaraman Nagar, Dindigul-624622, India
[3]Department of Electronics and Communication Engineering, Vel Tech Rangarajan Dr. Sagunthala R&D Institute of Science and Technology, Chennai-600062, India
[4]Department of Physics, Sri Eshwar College of Engineering, Kinathukadavu, Coimbatore-641202, India

*Corresponding authors: E-mail: senthilenvtce@gmail.com; sivakamitce@gmail.com

Received: 9 April 2026 *Accepted*: 16 June 2026 *Published online*: 7 August 2026 AJC-22428

This study reports the efficiency of continuous column adsorption for removal efficiency of benzene from aqueous solutions using thermally modified inorganic adsorbents. Brick powder (BP), granite powder (GP) and their composite mixture (BGM) were employed as adsorbent materials under varying thermal treatment conditions and column heights to assess their adsorption performance. Benzene concentrations of 5.56 mg/L, 3.10 mg/L and 1.28 mg/L were evaluated in a continuous flow system. The experimental data were analysed using the Thomas and Yoon-Nelson kinetic models to determine the rate constants (K_{TH} and K_{YN}) and the maximum solid-phase adsorption capacity (q_e). Thomas model exhibited excellent correlation with the experimental data, with regression coefficients (R^2) of 0.910, 0.980 and 0.976 for benzene concentrations of 5.56, 3.10 and 1.28 mg/L, respectively. Similarly, the Yoon-Nelson model showed strong agreement, with R^2 values of 0.998, 0.978 and 0.916 for the respective concentrations. XRD and SEM studies revealed that the thermal activation at elevated temperatures significantly enhanced the surface area and pore morphology of the adsorbents, transforming them from homogeneous to heterogeneous structures. The BP400 ºC column demonstrated the highest adsorption capacity and breakthrough efficiency, attributed to improved surface roughness and porosity. The results confirm that thermal modification improves the adsorption performance of both BP- and GP-based materials, making them suitable candidates for the removal of benzene and the treatment of contaminated water.

Keywords: Adsorption, Brick powder, Granite powder, Surface morphology, Kinetic study.

INTRODUCTION

Benzene is a volatile organic compound (VOC) widely used in industrial processes such as petrochemical refining, chemical manufacturing and polymer production. Its release through industrial effluents, chemical spills, storage tank leakage and landfill leachates has resulted in widespread environmental contamination. Long-term exposure to benzene can cause neurological disorders, hematological abnormalities and carcinogenic effect [1-3]. Occupational exposure remains a major concern for workers in industries such as rubber manufacturing, printing, steel production, shoe making, laboratory analysis and fuel handling [4,5]. Symptoms of acute exposure include dizziness, headaches, tremors and unconsciousness, while chronic exposure is associated with bone marrow suppression and an increased risk of leukemia. Consequently, benzene is classified as a Group 1 human carcinogen by the International Agency for Research on Cancer (IARC) [6].

Benzene exposure is commonly assessed by monitoring its metabolites in blood or urine shortly after exposure [7]. Due to its persistence and toxicity, the removal of benzene from contaminated water has become an important environmental challenge [8]. Among the available treatment methods, adsorption is considered one of the most efficient and cost-effective approaches for removing benzene and other aromatic pollutants from aqueous systems [9,10].

Although many studies have investigated benzene removal using low-cost adsorbents, most have focused on batch adsorption systems and individual adsorbent materials, with limited attention given to continuous fixed-bed operation and the effect of thermal activation [11-14]. The present study addresses this gap through a systematic investigation of benzene adsorption under continuous-flow conditions using construction waste-derived silicate materials, namely BP, GP and BGM (80% BP + 20% GP). A comparative evaluation of thermally activated adsorbents prepared at 100 ºC and 400 ºC was carried out under different influent benzene concentrations and column bed depths to assess breakthrough characteristics and adsorption kinetics. The experimental data were analysed using the Bohart-Adams, Thomas and Yoon-Nelson models, together with regeneration studies and structural characterisation, to evaluate the potential of thermally modified construction waste as a sustainable and cost-effective adsorbent for the treatment of benzene-contaminated water. Thermal activation at elevated temperatures improved the surface morphology and pore structure of the silicate-based adsorbents, leading to enhance the adsorption performance.

EXPERIMENTAL

Analytical-grade benzene (99.7% purity) and other solvents as well as chemicals obtained from Merck was used for adsorption studies. Sulphuric acid was served as the supporting electrolyte, while deionised water and HPLC-grade methanol were used as solvents. Benzene stock solutions (500 mg L^{-1}) were prepared and diluted to 5.56, 3.10 and 1.28 mg L^{-1} for adsorption experiments.

Preparation of column material: Brick powder (BP), granite powder (GP) and their blended mixture (BGM) were collected from local construction waste and utilised as low-cost silicate-based adsorbents for the removal of benzene from aqueous solutions. The raw materials were repeatedly washed with demineralised water to eliminate adhering dust, soil and impurities. Their adsorption capability is mainly attributed to the negatively charged silicate mineral surfaces, which enhance interactions with aromatic organic pollutants such as benzene. After cleaning and drying, the materials were subjected to thermal pre-treatment at 100 ºC for 2 h in a hot air oven and at 400 ºC for 3 h in a muffle furnace to improve surface activation, pore formation and adsorption efficiency. The treated adsorbents were sieved through a 4.76 mm mesh to obtain uniform particle size distribution. Prior to adsorption studies, the adsorbents were pre-treated with NaCl solution followed by washing with distilled water and drying at 80 ºC [15]. The Na^+ saturation process enhanced the cation exchange capacity and surface reactivity of the materials. Continuous-flow adsorption experiments were carried out using a glass column of 20 mm internal diameter packed with BP, GP or BGM at bed depths of 5, 8 and 11 cm. Benzene solutions with concentrations of 5.56, 3.10 and 1.28 mg/L were used as influent feed solutions to evaluate breakthrough behaviour and removal efficiency.

Preliminary optimisation studies were conducted using adsorbent particles of approximately 70 µm average size to investigate the effects of particle size, adsorbent dosage and contact time under controlled pH and flow conditions [16]. The results demonstrated that thermally activated BP, GP and BGM possess favourable physico-chemical characteristics for efficient benzene adsorption from aqueous media. The activation temperatures of 100 ºC and 400 ºC were selected to represent dehydration/conditioning and moderate thermal activation regimes, respectively.

Temperature of adsorbent: In this study, BP, GP and BGM were thermally treated at 100 ºC and 400 ºC to evaluate temperature-dependent adsorption behaviour [16]. The maximum improvement was observed at 400 ºC.

High pressure liquid chromatography (HPLC): A Shimadzu HPLC system (SPD-M20A, LC-20AT) equipped with Class VP software was employed for chromatographic measurements. A 500 mg L^{-1} benzene standard solution was prepared from a stock solution using acetonitrile. All reagents used were of HPLC grade and solutions were stored at 4 ºC in Amber bottles to prevent photodegradation [17]. Fresh standards were prepared daily with HPLC-grade water. A 20 µL sample volume was injected for analysis with a total runtime of 20 min. Benzene concentrations were quantified using retention time comparison and calibration curve analysis. The concentration of benzene in the treated samples was determined according to eqn. 1:

$$\text{Benzene concentration} = \frac{\text{Area of the peak in sample} \times \text{Concentration of standard solution}}{\text{Area of peak in standard solution}} \quad (1)$$

Adsorption modelling

Bohart-Adams (BM) model: The Bohart-Adams model is widely used to evaluate the breakthrough behaviour and dynamic performance of continuous fixed-bed adsorption columns. It relates influent and effluent concentrations, while break-through curves provide information on adsorption kinetics, mass transfer and adsorbent saturation [18]. The model is useful for evaluating adsorbent performance and optimising the design and operating conditions of large-scale adsorption systems. The model is defined by eqn. 2:

$$\text{BM} = \frac{\text{Treatment efficiency at a time interval (mg/L)}}{\text{Initial concentration of the influent (mg/L)}} \quad (2)$$

Thomas model: The Thomas model is widely used to predict adsorption behaviour in continuous fixed-bed columns. Based on Langmuir kinetics, it relates solute concentration to time and is used to determine the maximum adsorption capacity (q_o) and Thomas rate constant (K_{TH}). The model accounts for external film and internal pore diffusion, enabling the evaluation of adsorption kinetics and breakthrough behaviour for the removal of benzene [19]. The mathematical expression of the model is given in eqn. 3:

$$\ln\left(\frac{C_o}{C_t} - 1\right) = \left(K_{TH} \times q \times \frac{m}{Q}\right) - kt \times C_o \times t \quad (3)$$

where m is the mass of the adsorbent, C_o and C_t are the influent and effluent concentrations (mg/L), K_{TH} is the Thomas rate constant (mL/(min·mg) and t is the duration (min), The quantity of adsorbent in the column was measured as Q (g) and the adsorption kinetics (kt) were calculated from the plot of ln [(C_o/C_t)] over time for a constant flow rate.

Yoon-Nelson model: The Yoon-Nelson model describes adsorption in fixed-bed columns based on the probability of adsorbate adsorption and breakthrough [20]. The model estimates the rate constant (K_{YN}) and the time required for 50% breakthrough (τ), providing a simple approach to evaluate adsorption kinetics and column performance.

$$\ln\frac{C_t}{C_o - C_t} = K_{YN} - \tau \quad (5)$$

where the time reach for 50% of the adsorption break through (min), K_{YN} is the adsorption rate constant (1/min) and t is the time (min).

Column regeneration: The adsorption column was regenerated to restore the adsorption capacity of BP, GP and BGM for reuse. Spent adsorbents were washed with distilled water and NaCl solution to remove retained benzene and impurities [21], followed by air drying for 8 h before subsequent adsorption cycles.

Characterisation: The structural, morphological, functional and elemental properties of BP, GP and BGM before and after benzene adsorption were characterised using X-ray diffraction (XRD), scanning electron microscopy (SEM), Fourier transform infrared spectroscopy (FTIR) and scanning electron microscopy coupled with energy-dispersive X-ray analysis (SEM-EDAX). XRD was performed under 2θ geometry with a step size of 0.019º to examine the crystalline phases and structural changes. SEM was employed to investigate the surface morphology and pore structure, while FTIR spectra were recorded in the range of 4000-400 cm^{-1} using the KBr pellet method. SEM–EDAX analysis was carried out to evaluate the elemental composition and its distribution before and after adsorption. The combined characterisation techniques were used to assess the effect of thermal activation and benzene adsorption on the physico-chemical properties of the adsorbents.

RESULTS AND DISCUSSION

In this work, four adsorbent systems were investigated in the fixed-bed column experiments: (i) BP heated at 100 ºC, (ii) BGM consisting of 80% BP and 20% GP heated at 100 ºC, (iii) BP heated at 400 ºC and (iv) BGM consisting of 80% BP and 20% GP heated at 400 ºC. The adsorption performances of these materials were evaluated at influent benzene concentrations of 5.56, 3.10 and 1.28 mg/L using column heights of 5, 8 and 11 cm under an inlet flow rate of 2.5 mL/min. The corresponding adsorption efficiencies, breakthrough times and flow characteristics are shown in Table-1.

Effect of temperature and column height on benzene adsorption performance: Fixed-bed adsorption experiments were carried out using brick powder (BP) and granite powder composite (BGM; 80% BP + 20% GP) at influent benzene concentrations of 5.56, 3.10 and 1.28 mg/L to examine the role of thermal activation and bed depth on adsorption behaviour. The adsorption response varied with influent concentration, activation temperature and hydrodynamic conditions within the packed bed. Variations in the break-through time, adsorption efficiency and outlet flow rate reflected changes in pore accessibility, surface activity and mass-transfer characteristics of the adsorbents [22].

Influence of thermal activation temperature on adsorption efficiency: The thermal treatment applied to the adsorbents governed the development of adsorption sites and pore structure. Activation at 400 ºC produced materials with higher adsorption activity than those treated at 100 ºC, owing to the removal of residual volatile matter and the formation of additional micro- and mesopores within the silicate matrix [23]. The increase in surface energy and accessible pore volume strengthened the interaction between benzene molecules and the adsorbent surface through van der Waals forces and π-π interactions [24].

At an influent concentration of 5.56 mg/L, BP heated at 400 ºC exhibited initial adsorption efficiencies of 0.295, 0.673 and 0.732 mg/L for column heights of 5, 8 and 11 cm, respectively. The corresponding values for BP activated at 100 ºC were lower, reaching 0.313 mg/L only at the 5 cm bed depth. The BGM composite activated at 400 ºC produced adsorption efficiencies of 0.105, 0.425 and 0.519 mg/L, while the composite treated at 100 ºC reached 0.112, 0.291 and 0.097 mg/L for the same column height.

TABLE-1
CONTINUOUS ADSORPTION STUDY FOR HIGH ADSORPTION EFFICIENCY FOR BENZENE AT DIFFERENT CONCENTRATIONS

Set	Adsorbent type/heating condition	Column height (cm)	Inlet flow (mL/min)	Outlet flow (mL/min)	Initial efficiency (mg/L)			Breakthrough/ Exhaustion time (min)			Final high adsorption efficiency (mg/L)		
					5.56 mg/L	3.10 mg/L	1.28 mg/L	5.56 mg/L	3.10 mg/L	1.28 mg/L	5.56 mg/L	3.10 mg/L	1.28 mg/L
1	BP heated at 100 ºC (Hot air oven, 2 h)	5	2.5	0.50	0.313	0.110	0.230	2000	400	240	5.56	3.10	1.28
		8	2.5	0.42	–	–	–	1160	360	220	5.56	3.10	1.28
		11	2.5	0.37	–	–	–	1060	380	200	5.56	3.10	1.28
2	BP 80% + GP 20% heated at 100 ºC	5	2.5	0.40	0.112	0.210	0.140	2000	380	200	5.56	3.10	1.28
		8	2.5	0.35	0.291	0.260	0.270	1180	460	140	5.56	3.10	1.28
		11	2.5	0.30	0.097	0.090	0.390	1160	440	120	5.56	3.10	1.28
3	BP heated at 400 ºC (Muffle furnace)	5	2.5	0.60	0.295	0.820	0.390	1160	360	180	5.56	3.10	1.28
		8	2.5	0.50	0.673	0.830	0.510	1060	320	140	5.56	3.10	1.28
		11	2.5	0.40	0.732	0.930	0.840	920	260	100	5.56	3.10	1.28
4	BP 80% + GP 20% heated at 400 ºC	5	2.5	0.50	0.105	0.100	0.060	2000	480	240	5.56	3.10	1.28
		8	2.5	0.45	0.425	0.580	0.060	1160	460	220	5.56	3.10	1.28
		11	2.5	0.40	0.519	0.630	0.060	1060	440	200	5.56	3.10	1.28

The influence of activation temperature became more pronounced at an influent concentration of 3.10 mg/L. BP activated at 400 ºC achieved adsorption capacities of 0.820, 0.830 and 0.930 mg/g at bed heights of 5, 8 and 11 cm, respectively, compared with 0.110 mg/g for BP treated at 100 ºC under identical operating conditions [25,26]. The BGM composite activated at 400 ºC exhibited adsorption capacities between 0.100 and 0.630 mg/g, whereas the corresponding material treated at 100 ºC exhibit values between 0.090 and 0.260 mg/g. At the lowest influent concentration of 1.28 mg/L, BP activated at 400 °C reached adsorption efficiencies of 0.390, 0.510 and 0.840 mg/L for column heights of 5, 8 and 11 cm, respectively. BP heated at 100 ºC exhibit a maximum value of 0.230 mg/L at 5 cm [27,28]. The BGM composite activated at 100 ºC yielded adsorption efficiencies of 0.140, 0.270 and 0.390 mg/L, whereas the corresponding composite heated at 400 ºC maintained values close to 0.060 mg/L throughout the investigated bed depths. Thus, the adsorption data obtained at all three influent concentrations identify 400 °C as the most favourable activation temperature for enhancing benzene uptake by both BP and BGM through improvement of pore structure and surface activity [25].

Effect of column height and flow rate: The inlet flow rate remained constant at 2.5 mL/min throughout the study, whereas the outlet flow rate varied between 0.60 and 0.30 mL/min depending on the bed depth and adsorbent composition. The reduction in outlet flow with increasing column height originated from the larger hydraulic resistance developed by the packed bed [29].

For the influent concentration of 5.56 mg/L, outlet flow rates decreased from approximately 0.50-0.60 mL/min at the 5 cm bed to 0.30-0.40 mL/min at the 11 cm bed. BP activated at 100 ºC produced exhaustion times of 2000, 1160 and 1060 min for bed heights of 5, 8 and 11 cm, respectively, while BP activated at 400 ºC reached 1160, 1060 and 920 min. BGM activated at 400 ºC recorded exhaustion times of 2000, 1160 and 1060 min for the corresponding column heights [30]. At an influent concentration of 3.10 mg/L, BP activated at 400 ºC exhibited breakthrough times of 360, 320 and 260 min with increasing bed depth from 5 to 11 cm [31]. The BGM composite activated at 400 °C exhibited breakthrough times of 480, 460 and 440 min for bed heights of 5, 8 and 11 cm, respectively, which may be attributed to the more uniform distribution and accessibility of adsorption sites within the composite structure [32]. BP treated at 100 ºC reached breakthrough times of 400, 360 and 380 min, whereas BGM activated at 100 ºC yielded values of 380, 460 and 440 min.

At 1.28 mg/L, BP activated at 400 ºC exhibited exhaustion times of 180, 140 and 100 min at bed heights of 5, 8 and 11 cm, respectively. The corresponding BP material treated at 100 ºC remained operational for 240, 220 and 200 min, reflecting slower adsorption kinetics and diffusion-controlled transport within the less active adsorbent matrix [33]. BGM activated at 100 ºC produced breakthrough times of 200, 140 and 120 min, while the composite treated at 400 ºC maintained breakthrough times of 240, 220 and 200 min. The reduction in breakthrough time observed in some of the deeper beds may be associated with the rapid occupation of highly active sites generated during thermal activation, resulting in steeper breakthrough curves and a narrower mass-transfer zone despite the increase in adsorbent mass [34].

Comparative performance of BP and BGM: Differences between BP and BGM became evident across the three influent concentrations and activation conditions. The addition of 20% GP improved the structural integrity of the adsorbent bed and provided a more uniform pore network, contributing to greater hydraulic stability during continuous operation [30, 32]. At 5.56 mg/L, BGM activated at 400 ºC achieved breakthrough times between 1060 and 2000 min, accompanied by adsorption efficiencies ranging from 0.105 to 0.519 mg/L. BP activated at 400 ºC reached higher instantaneous adsorption efficiencies, attaining 0.732 mg/L at the 11 cm bed depth, although saturation occurred more rapidly.

For the influent concentration of 3.10 mg/L, BP activated at 400 ºC exhibited adsorption capacities between 0.820 and 0.930 mg/g, while BGM activated at 400 ºC maintained capacities between 0.100 and 0.630 mg/g together with breakthrough times extending to 480 min. The BP material favoured rapid benzene uptake, whereas the composite favoured longer column operation. At 1.28 mg/L, BP activated at 400 ºC shows the highest adsorption efficiency of 0.840 mg/L at the 11 cm column height. The BGM composite maintained more stable breakthrough behaviour across the investigated bed depths and thermal conditions, which may be attributed to the beneficial contribution of GP to pore connectivity and flow distribution within the packed bed [32].

Thus, the effluent benzene concentration approached the influent values of 5.56, 3.10 and 1.28 mg/L at column exhaustion confirmed the achievement of adsorption equilibrium under the selected operating conditions. Among the studied absorbents, BP favoured higher adsorption rates and capacities, whereas BGM provided better operational stability during prolonged continuous adsorption experiments.

X-ray diffraction study: The X-ray diffraction (XRD) patterns of the powdered adsorbents before and after benzene adsorption are shown in Fig. 1. The diffraction profiles confirm the presence of mineral phases associated with construction waste-derived materials, primarily silica, iron oxide, alumina and magnesia. All adsorbents exhibited partially ordered to predominantly amorphous structures. Benzene adsorption caused changes in peak intensity and slight peak broadening without the appearance of new diffraction peaks, confirmed that no new crystalline phases were formed during adsorption. BP400 exhibited sharper diffraction peaks than BP100, reflecting improved structural ordering after thermal activation. Similar behaviour was observed for the BGM composite, where BGM400 exhibited a more defined diffraction pattern than BGM100. The reduction in peak intensity after adsorption can be attributed to surface coverage by benzene molecules and minor structural perturbations, while the persistence of the characteristic diffraction peaks confirms the structural stability of the adsorbents throughout the adsorption process [35,36]. The XRD analysis was limited to qualitative structural assessment as JCPDS/PDF card matching and quantitative crystallinity analysis were not performed.

SEM studies of packed column material: SEM was employed to examine the surface morphology of the sorbents before and after benzene adsorption (Fig. 2). Prior to adsorp-

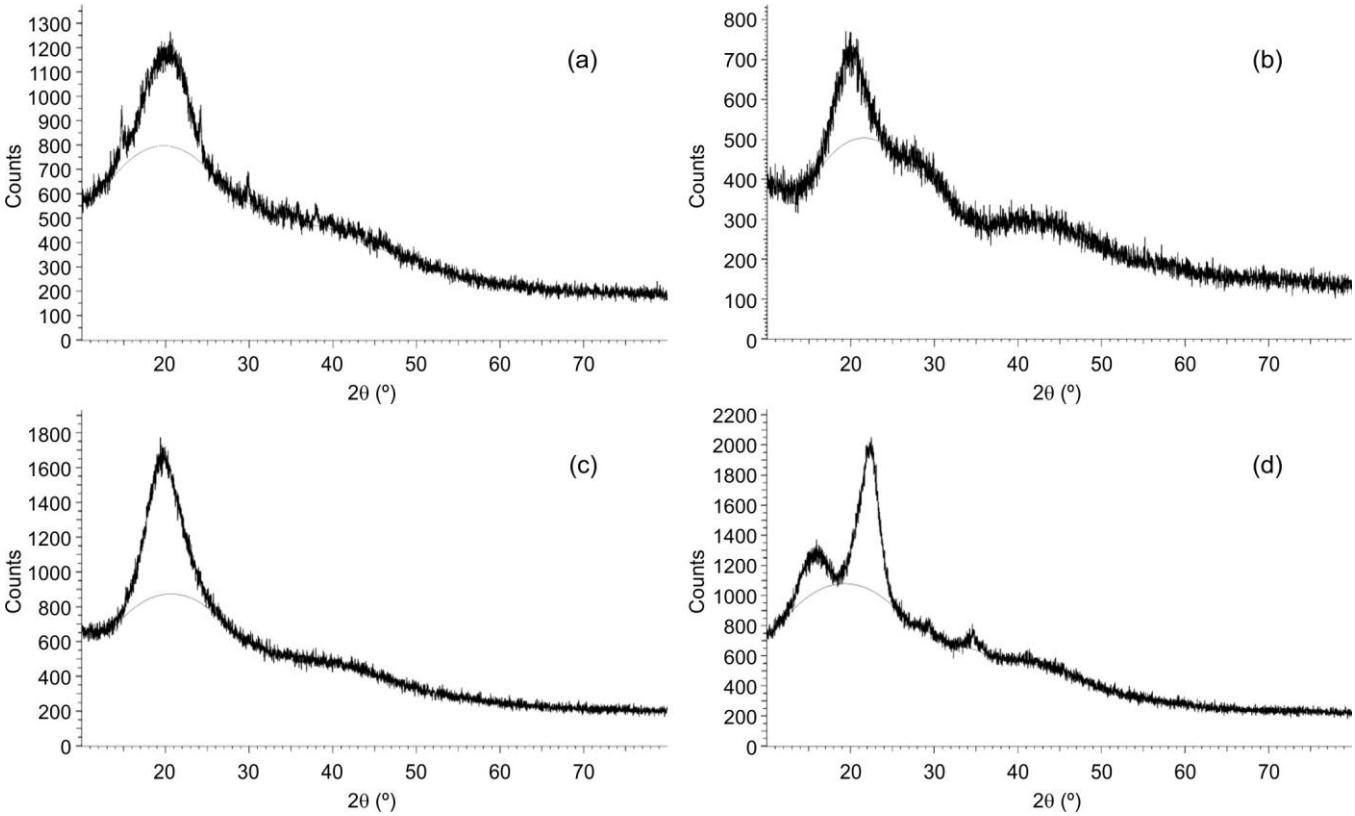

Fig. 1. XRD patterns of (a) BP 100, (b) BP80% + GP20% 100, (c) BP 400 and (d) BP80% + GP20% 400

tion, all sorbents exhibited relatively compact and continuous surfaces with limited surface irregularities and fewer discernible pores. Such morphological characteristics are typical of thermally treated silicate-based adsorbents before exposure to organic contaminants. After benzene adsorption, the surface appearance changed appreciably. The SEM images display petal-like surface features accompanied by interconnected micron-sized channels, irregular cavities and enlarged voids [37]. These features exhibit a rougher and more heterogeneous surface compared with the corresponding pristine materials.

The development of channels and cavities is consistent with the accessibility of the pore network during adsorption. Interaction of benzene molecules with the adsorbent surface may promote local rearrangement of surface particles and expose previously inaccessible regions within the porous framework. The resulting increase in surface irregularity is associated with a larger number of accessible adsorption sites and higher textural heterogeneity, both of which favour mass transfer during adsorption.

FTIR analysis: Fourier transform infrared (FTIR) spectroscopy was employed to investigate the surface functional groups of the sorbents before and after benzene adsorption, providing insight into the adsorption mechanism (Fig. 3). It had amino, carboxyl, sulphonate and hydroxyl groups. Around 3421 cm^{-1}, OH and NH groups showed a wide and pronounced absorption. In the absorption band at 1633 cm^{-1}, C=O stretch is primarily shown. COH could be the source of bands at 1043 cm^{-1}. The internal reaction of the sorbent was clearly visible in the FTIR spectra of BP-100, BGM100, BP-400 and BGM-400 following sorption [38]. The large peak in BP100 at 2347.35 cm^{-1} was attributed to benzene groups and the elongating vibration of H_2O molecules in the pattern. The elongating vibration of the N_2 groups of water that were taken in from the surrounding environment coincided with the deformation peak at 777.31 cm^{-1}. The characteristic stretching vibrations for alumina oxide and iron oxide bonds were investigated at 694.37 cm^{-1} and group bending modes were observed between 459.06 and 580.57 cm^{-1} [39]. After benzene adsorption, the FTIR spectra of fully exhausted columns revealed notable modifications in the column contents.

The large peak in BGM100 at 1049.28 cm^{-1} was attributed to benzene groups and the elongating vibration of H_2O molecules in the pattern. The elongated vibration of the N_2 groups of water received from the environment outside was associated with the deformation peak at 777.16 cm^{-1} [40]. Possible carbonyl or amide group C=O bonds may be found within a radius of 2347.37 cm^{-1} and group bending modes could be seen between 582.50 and 644.22 cm^{-1}. The large peak of 1047.35 cm^{-1} in BP400 was linked to benzene groups and the pattern's elongating vibration of water molecules. The elongating vibration of N_2 groups of water received from the external environment coincided with the deformation peak at 775.38 cm^{-1}. Possible carbonyl or amide group C=O bonds may be found within a radius of 2347.37 cm^{-1} and group bending modes could be observed between 582.50 and 644.22 cm^{-1}. The broad peak of 1041.56 cm^{-1} in BGM400 is attributable to C=O. The peak at 1629 cm^{-1} could be attributed to polysaccharide C-O stretching [41]. The elongating vibration of N_2 groups of water received from the external environment coincided with the deformation peak at 775.38 cm^{-1}. Possible

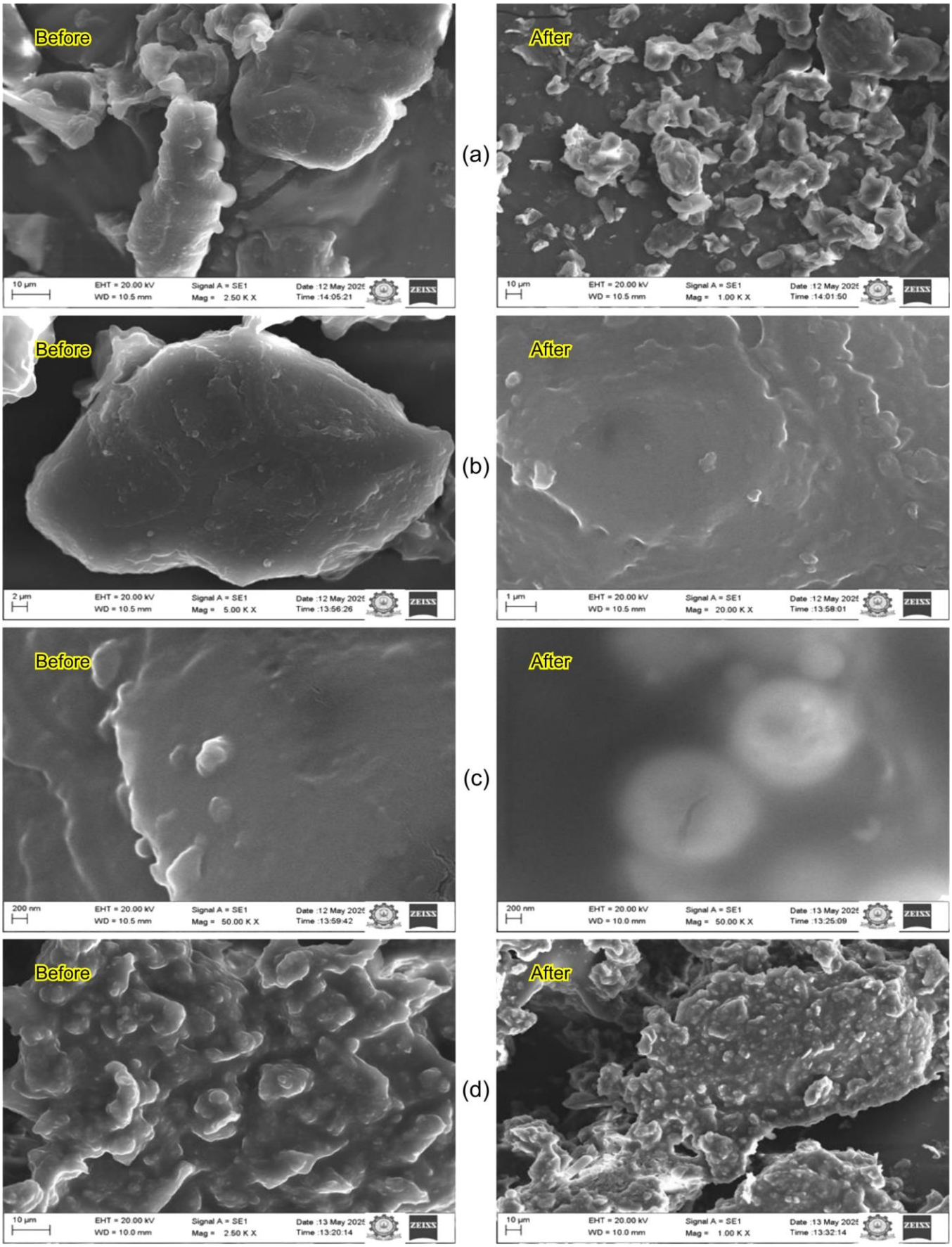

Fig. 2. SEM images of (a) BP 100, (b) BP80% + GP20% 100, (c) BP 400 and (d) BP80% + GP20% 400 before and after treatment

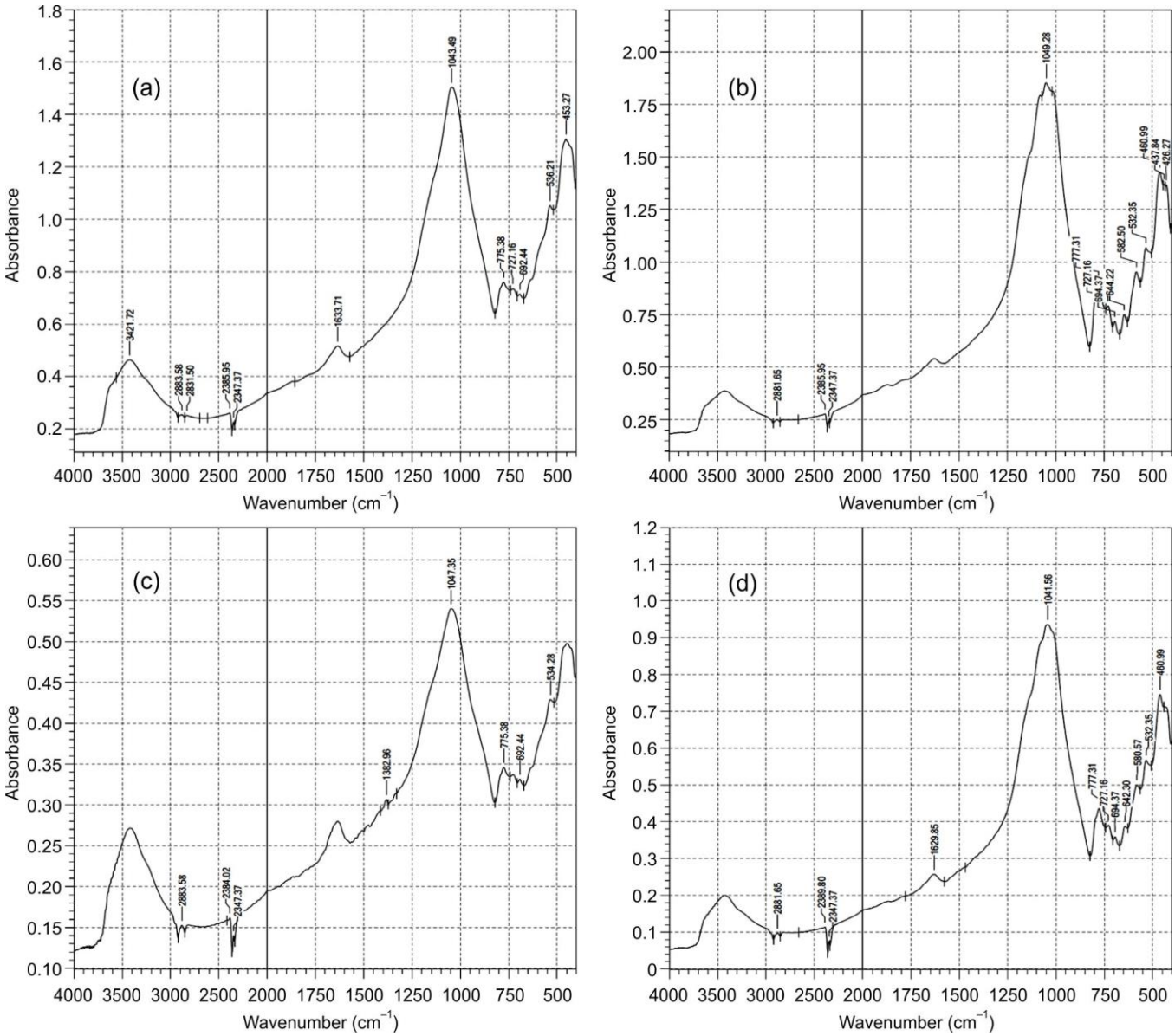

Fig. 3. FTIR spectra of (a) BP 100, (b) BP80% + GP20% 100, (c) BP 400 and (d) BP80% + GP20% 400

–OH (carboxylic acid) peak at 2347.37 cm^{-1} and group bending modes between 582.50 and 644.22 cm^{-1} were observed.

SEM-EDAX studies: SEM–EDAX analysis of BP100, BGM100, BP400 and BGM400 was performed to examine the surface morphology and elemental composition of the prepared adsorbents. SEM micrographs (Fig. 4) revealed irregular, rough and porous surfaces with interconnected pores and micro-cavities. Thermal treatment at 400 ºC produced a more developed surface texture than that observed at 100 ºC improving pore accessibility for benzene diffusion. The incorporation of 20% granite powder produced a more heterogeneous surface morphology with a higher diversity of accessible adsorption sites. EDAX spectra (Fig. 4) confirmed the presence of oxygen (O), silicon (Si), calcium (Ca), potassium (K), sulfur (S), phosphorus (P), magnesium (Mg), carbon (C) and nitrogen (N), together with trace amounts of copper (Cu) and lead (Pb), characteristic of silicate-based materials [42]. The dominant oxygen and silicon signals confirmed the oxide-rich silicate framework, while the higher silicon content in the brick-granite composites reflected the contribution of silica-rich granite minerals, which enhance the structural stability of the adsorbents [43]. Trace quantities of Cu and Pb were attributed to naturally occurring mineral impurities or background signals during EDAX analysis [44].

Bohart–Adams adsorption study: The Bohart-Adams model was used to evaluate the breakthrough behaviour of benzene by relating the influent and effluent benzene concentrations during fixed-bed adsorption. The model was applied at influent benzene concentrations of 5.56, 3.10 and 1.28 mg/L to examine the dynamic performance of the adsorption column under different operating conditions [45]. The 11 cm BP column activated at 400 ºC exhibited the highest adsorption performance, achieving complete removal of benzene at an influent concentration of 5.56 mg/L within 920 min. At influent concentrations of 3.10 and 1.28 mg/L, complete benzene removal

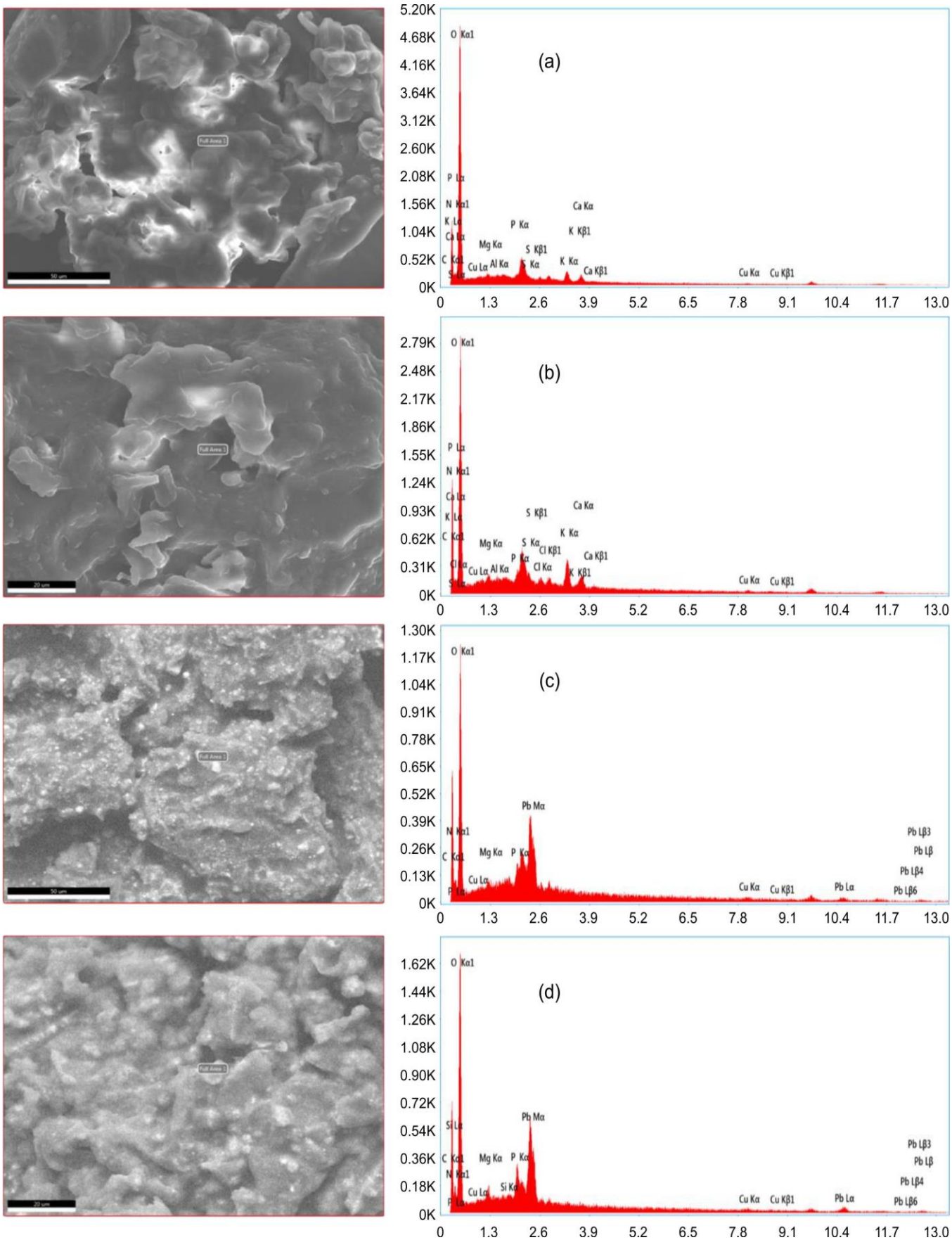

Fig. 4. SEM-EDAX spectra of (a) BP 100, (b) BP80% + GP20% 100, (c) BP 400 and (d) BP80% + GP20% 400

was achieved within 260 and 100 min, respectively. The improved performance can be attributed to the development of a porous structure and a higher number of accessible adsorption sites following thermal activation. The BP-GP composite (80:20) activated at 400 ºC exhibited lower adsorption performance, which may be attributed to reduced pore accessibility within the mixed material matrix [46]. The Bohart-Adams model closely matched the experimental breakthrough curves (Fig. 5).

Thomas model adsorption studies: The Thomas model was used to evaluate the adsorption kinetics of benzene in fixed-bed columns packed with BP and BGM under different thermal activation conditions. The Thomas rate constant (K_{TH}), maximum adsorption capacity (q_o) and coefficient of determination (R^2) obtained from the model are presented in Table-2 for influent benzene concentrations of 5.56, 3.10 and 1.28 mg/L, respectively [45,47].

Across all the studied conditions, the model provided satisfactory agreement with the experimental data, with R^2 values ranging from 0.775 to 0.993, confirm its suitability for describing benzene adsorption in fixed-bed columns [48-50]. At 100 ºC, BP exhibited adsorption capacities (q_o) of 19.08-1.512, 2.10-4.60 and 0.392-0.970 mg/g for influent concentrations of 5.56, 3.10 and 1.28 mg/L, respectively, while the corresponding K_{TH} values varied from 1.4×10^{-5}–2.9×10^{-5}, 2.0×10^{-5}–13.1×10^{-5} and 0.357–0.440 $\times 10^{-3}$ mL/min/mg [48,50,51]. Under the same conditions, the BGM composite exhibited q_o values of 15.78-19.33, 2.35-5.37 and 0.756-2.455 mg/g, with R^2 values ranging from 0.866 to 0.979, which are consistent with stable adsorption behaviour across the investi-

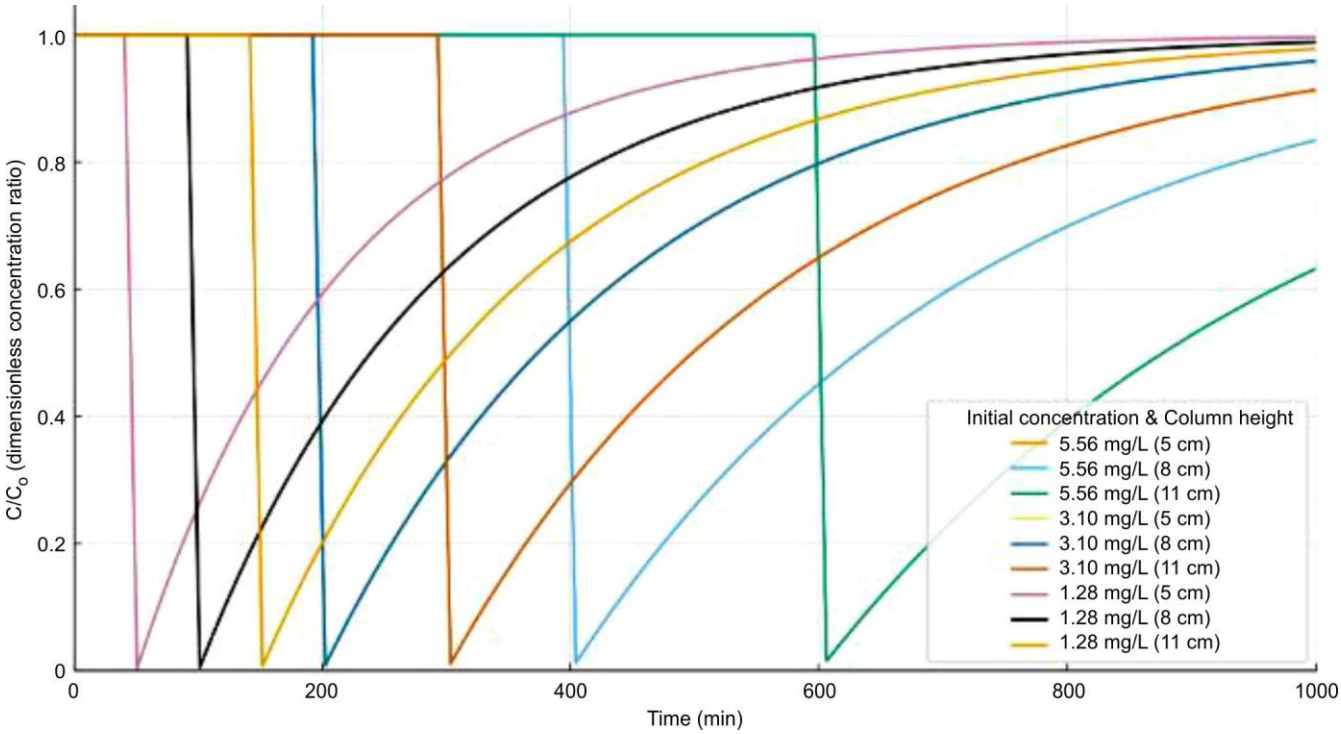

Fig. 5. Breakthrough curves on benzene adsorption at different concentrations by Bohart–Adams model

TABLE-2
VALIDATION OF THOMAS MODEL AT DIFFERENT CONCENTRATIONS, Q = 2.5 mL/min

Material	Column size (cm)	$k_t \times 10^{-3}$ (mL/(min mg))			q_o (mg/g)			R^2		
		5.56 mg/L	3.10 mg/L	1.28 mg/L	5.56 mg/L	3.10 mg/L	1.28 mg/L	5.56 mg/L	3.10 mg/L	1.28 mg/L
BP-100	5	0.015	0.131	0.381	19.08	4.35	0.970	0.910	0.993	0.966
	8	0.029	0.020	0.440	0.40	4.60	0.896	0.929	0.963	0.984
	11	0.014	0.067	0.357	1.512	2.10	0.392	0.954	0.919	0.976
BP 80% + GP20% (BGM-100)	5	0.016	0.133	0.323	19.33	4.21	1.345	0.922	0.948	0.878
	8	0.015	0.110	0.319	17.80	5.37	0.756	0.919	0.775	0.979
	11	0.016	0.030	0.134	15.78	2.35	2.455	0.929	0.922	0.866
BP-400	5	0.014	0.032	0.382	12.34	6.80	0.572	0.922	0.919	0.859
	8	0.011	0.086	0.106	14.49	3.62	2.749	0.943	0.958	0.956
	11	0.006	0.141	0.067	0.008	3.65	1.246	0.985	0.971	0.981
BP 80% + GP20% (BGM-400)	5	0.018	0.050	0.465	18.03	6.28	0.748	0.985	0.918	0.903
	8	0.012	0.030	0.465	17.91	7.92	0.656	0.973	0.880	0.826
	11	0.008	0.062	0.596	10.02	3.22	0.866	0.993	0.973	0.123

gated concentrations [22,51]. Thermal activation at 400 ºC altered the adsorption characteristics of both adsorbents. For BP, the maximum adsorption capacities were 12.34, 6.80 and 2.749 mg/g at influent concentrations of 5.56, 3.10 and 1.28 mg/L, respectively, whereas the corresponding BGM composite exhibited q_o values of 10.02-18.03, 3.22-7.92 and 0.656-0.866 mg/g [52-54]. The BGM composite produced the highest model correlation (R^2 = 0.973-0.993) at 5.56 mg/L, while the lowest value (R^2 = 0.123) was obtained for the 11 cm column at 1.28 mg/L, which may be associated with non-uniform flow distribution within the packed bed [55]. The variation in q_o and K_{TH} with influent concentration, thermal activation and bed height reflects changes in adsorption kinetics, pore accessibility and mass-transfer behaviour during fixed-bed operation.

Yoon–Nelson model for adsorption study: The Yoon-Nelson model parameters obtained for influent benzene concentrations of 5.56, 3.10, and 1.28 mg/L are shown in Table-3. The model constants like the rate constant (K_{YN}), characteristic time (τ) and coefficient of determination (R^2), were used to evaluate the breakthrough behaviour of benzene under different thermal activation conditions and column heights. Across all operating conditions, R^2 values ranged from 0.064 to 0.998, confirming satisfactory agreement between the experimental and predicted breakthrough curves for most adsorption systems. For BP activated at 100 ºC, K_{YN} values ranged from 0.045-0.075, 0.027-0.126 and 0.006-0.581 min^{-1} at influent concentrations of 5.56, 3.10 and 1.28 mg/L, respectively, while the corresponding τ values remained within 8.6-8.8 h, ≈10 h and 2.33-2.92 h [56-58]. The BGM composite activated at 100 ºC exhibited K_{YN} values of 0.062-0.087, 0.062-0.087 and 0.196-0.489 min^{-1}, with τ values ranging from 8.4-9.0 h, 7.1-7.3 h and 2.34-2.60 h, respectively. The corresponding R^2 values (0.769-0.979) indicate satisfactory model fitting despite minor deviations attributed to surface heterogeneity and pore accessibility [59,60]. Thermal activation at 400 ºC increased the adsorption rate constants for both adsorbents. BP exhibited K_{YN} values of 0.067-0.072, 0.332-0.366 and 0.510-0.529 min^{-1}, while the corresponding τ values decreased from 8.48-8.74 h to 7.0-7.4 h and 1.48-1.86 h as the influent concentration decreased. The associated R^2 values reached 0.998, indicating excellent agreement between the model and the experimental data [61-63]. The thermally activated BGM composite exhibited K_{YN} values of 0.067-0.094, 0.140-0.255 and 0.563-0.769 min^{-1}, with τ values of 8.48-8.74 h, 7.1-7.6 h and 2.26-2.86 h, respectively. Most experimental data were well represented by the model (R^2 = 0.826-0.981), although the 11 cm BP column at 1.28 mg/L exhibited a lower R^2 value (0.064), which may be attributed to non-uniform flow distribution within the packed bed [58]. The increase in K_{YN} and the corresponding reduction in τ after thermal activation indicates faster adsorption kinetics and earlier breakthrough, which can be attributed to improved pore development and better accessibility of active adsorption sites.

Comparison of the Bohart-Adams, Thomas and Yoon-Nelson models revealed that the Thomas and Yoon-Nelson models consistently produced higher R^2 values and better agreement with the experimental breakthrough curves, whereas the Bohart-Adams model exhibited lower fitting accuracy for some operating conditions, particularly over the complete breakthrough profile. These observations support the applicability of the Thomas and Yoon-Nelson models for predicting benzene adsorption in continuous fixed-bed columns.

Conclusion

A continuous fixed-bed column was employed to evaluate benzene adsorption using brick powder (BP), granite powder (GP) and brick-granite composite (BGM) adsorbents at bed depths of 5, 8 and 11 cm and influent benzene concentrations of 1.28, 3.10 and 5.56 mg/L. The adsorbents exhibited effective benzene removal under the studied conditions, with adsorption performance improving as bed depth increased. The breakthrough data were satisfactorily described by the Bohart-Adams, Thomas and Yoon–Nelson models, which confirmed the applicability of these models for predicting fixed-bed adsorption behaviour. Thermal activation at 400 ºC enhanced the adsorption performance by modifying the surface morphology and pore structure of the adsorbents, which is consistent with the SEM and XRD characterisation results.

TABLE-3
PARAMETERS OF YOON-NELSON MODEL AT DIFFERENT CONCENTRATIONS

Material	Column size (cm)	k_y (min^{-1})			τ (h)			R^2		
		5.56 mg/L	3.10 mg/L	1.28 mg/L	5.56 mg/L	3.10 mg/L	1.28 mg/L	5.56 mg/L	3.10 mg/L	1.28 mg/L
BP-100	5	0.075	0.087	0.488	8.83	10.16	2.92	0.961	0.919	0.976
	8	0.062	0.126	0.581	8.67	10.04	2.74	0.924	0.600	0.980
	11	0.045	0.027	0.006	8.65	10.92	2.33	0.941	0.980	0.064
BGM-100	5	0.087	0.087	0.196	9.02	7.12	2.60	0.925	0.775	0.834
	8	0.062	0.062	0.409	8.66	7.18	2.42	0.903	0.769	0.979
	11	0.074	0.074	0.489	8.42	7.33	2.34	0.938	0.769	0.976
BP-400	5	0.067	0.345	0.510	7.58	7.38	1.86	0.949	0.925	0.982
	8	0.068	0.366	0.529	7.62	7.32	1.64	0.966	0.943	0.986
	11	0.072	0.332	0.529	7.60	7.04	1.48	0.998	0.978	0.916
BGM-400	5	0.094	0.140	0.769	8.74	7.62	2.86	0.973	0.952	0.957
	8	0.068	0.255	0.596	8.66	7.44	2.68	0.923	0.959	0.826
	11	0.067	0.195	0.563	8.48	7.12	2.26	0.907	0.911	0.981

Among the investigated materials, BP400 exhibited the best agreement with the Thomas model and the highest adsorption performance. These findings demonstrate that thermally activated construction waste-derived adsorbents offer an efficient, low-cost and sustainable approach for the continuous removal of benzene from contaminated water.

CONFLICT OF INTEREST

The authors declare that there is no conflict of interests regarding the publication of this article.

DECLARATION OF AI-ASSISTED TECHNOLOGIES

During the preparation of this manuscript, the authors used an AI-assisted tool(s) to improve the language and no data, results or scientific conclusions were generated by AI. All analyses, interpretations and conclusions are the authors' own. The authors reviewed and edited the content and take full responsibility for the published work.

REFERENCES

1. J.-C. Pu, M.D. Dari, X.-Q. Tang and P.-Q. Yuan, *Chem. Eng. Sci.*, **224**, 115793 (2020); https://doi.org/10.1016/j.ces.2020.115793
2. P. Kumari, D. Soni and S.G. Aggarwal, *Environ. Anal. Health Toxicol.*, **39**, e2024012 (2024); https://doi.org/10.5620/eaht.2024012
3. S.-B. Barbeș, A. Bărbulescu and L. Barbeș, *Toxics*, **12**, 187 (2024); https://doi.org/10.3390/toxics12030187
4. C.C. Bao, *J. Asian Multicult. Res. Med. Health Sci. Stud.*, **3**, 77 (2022); https://doi.org/10.47616/jamrmhss.v3i3.333
5. A.C. Capleton and L.S. Levy, *Chem.-Biol. Interact.*, **153-154**, 43 (2005); https://doi.org/10.1016/j.cbi.2005.03.007
6. American Cancer Society, Benzene and Cancer Risk, American Cancer Society, (2023); https://www.cancer.org/cancer/risk-prevention/chemicals/benzene.html (Accessed on March 5, 2026).
7. S.M. Arnold, J. Angerer, P.J. Boogaard, M.F. Hughes, R.B. O'Lone, S.H. Robison and A.R. Schnatter, *Crit. Rev. Toxicol.*, **43**, 119 (2013); https://doi.org/10.3109/10408444.2012.756455
8. L.M. Haupert, J. McDonnell, K. Martel, M.D. Miles and M.L. Magnuson, *J. Hazard. Mater. Adv.*, **3**, 100013 (2021); https://doi.org/10.1016/j.hazadv.2021.100013
9. F. Alshahrani, B. Tawabini, T. Saleh, M. Alrayaan, S. Alaama, R. Nasser, P. Soupios, P. Kirmizakis, M. Mahmoud, T. Oyehan and E. Safi, *Sci. Rep.*, **12**, 19651 (2022); https://doi.org/10.1038/s41598-022-24283-6
10. J. Choma, B. Szczęśniak, A. Kapusta and M. Jaroniec, *Molecules*, **29**, 5677 (2024); https://doi.org/10.3390/molecules29235677
11. R. Salehi, F. Dadashian, M. Abedi and A. Eliassi, *Heliyon*, **11**, e42071 (2025); https://doi.org/10.1016/j.heliyon.2025.e42071
12. K. Isinkaralar, *Molecules*, **28**, 3453 (2023); https://doi.org/10.3390/molecules28083453
13. F. Obiri-Nyarko, J. Kwiatkowska-Malina, S.K. Kumahor and G. Malina, *J. Contam. Hydrol.*, **250**, 104054 (2022); https://doi.org/10.1016/j.jconhyd.2022.104054
14. N. Baimatova, M. Derbissalin, A. Kabulov and B. Kenessov, *Eurasian Chem.-Technol. J.*, **18**, 123 (2016); https://doi.org/10.18321/ectj433
15. H. Lu, M. Qian, Q. Wang and Y. Yang, *J. Phys. Org. Chem.*, **33**, e4061 (2020); https://doi.org/10.1002/poc.4061
16. D. Zhang, J. Liu, M. Liu, L. Liu and D.D. Do, *Sep. Purif. Technol.*, **251**, 117306 (2020); https://doi.org/10.1016/j.seppur.2020.117306.
17. S. Hazrati, R. Rostami, M. Farjaminezhad and M. Fazlzadeh, *Atmos. Environ.*, **132**, 91 (2016); https://doi.org/10.1016/j.atmosenv.2016.02.042
18. M. Senthil Kumar, V. Sivasankar and G.V.T. Gopalakrishna, *Arab. J. Chem.*, **10**, S2523 (2017); https://doi.org/10.1016/j.arabjc.2013.09.022
19. C. Louis, Y. Liu, P. Tassel, P. Perret, A. Chaumond and M. Andre, *Atmos. Environ.*, **141**, 80 (2016); https://doi.org/10.1016/j.atmosenv.2016.06.055
20. C. Gonzalez-Galan, A. Luna-Triguero, J.M. Vicent-Luna, A.P. Zaderenko, A. Slawek, R. Sanchez-de-Armas and S. Calero, *Chem. Eng. J.*, **398**, 125678 (2020); https://doi.org/10.1016/j.cej.2020.125678
21. Y. Huang, Q. Cheng, Z. Wang, S. Liu, C. Zou, J. Guo and X. Guo, *Chem. Eng. J.*, **398**, 125557 (2020); https://doi.org/10.1016/j.cej.2020.125557
22. H. Amini, V. Hosseini, C. Schindler, H. Hassankhany, M. Yunesian, S.B. Henderson and N. Künzli, *Environ. Pollut.*, **226**, 219 (2017); https://doi.org/10.1016/j.envpol.2017.04.027
23. S. Zali, F. Jalali, A. Es-Haghi and M. Shamsipur, *J. Chromatogr. B Analyt. Technol. Biomed. Life Sci.*, **1033-1034**, 287 (2016); https://doi.org/10.1016/j.jchromb.2016.08.045.
24. N. Baimatova, B. Kenessov, J.A. Koziel, L. Carlsen, M. Bektassov and O.P. Demyanenko, *Talanta*, **154**, 46 (2016); https://doi.org/10.1016/j.talanta.2016.03.050
25. J. Dai, Y. Guo, L. Xu, G. Zhuang, Y. Zheng, D. Sun, J. Huang and Q. Li, *Mol. Catal.*, **486**, 110849 (2020); https://doi.org/10.1016/j.mcat.2020.110849
26. I. Akmirza, C. Pascual, A. Carvajal, R. Perez, R. Munoz and R. Lebrero, *Sci. Total Environ.*, **587-588**, 457 (2017); https://doi.org/10.1016/j.scitotenv.2017.02.130
27. S. Kweon, S. Lee, J.H. Lee and M.B. Park, *Appl. Surf. Sci.*, **612**, 155851 (2023); https://doi.org/10.1016/j.apsusc.2022.155851
28. L. Zhao, X. Deng, J. Gao and Y. Ma, *Inorg. Chim. Acta*, **544**, 121227 (2023); https://doi.org/10.1016/j.ica.2022.121227
29. Y. Ji, F. Gao, Z. Wu, L. Li, D. Li, H. Zhang, Y. Zhang, J. Gao, Y. Bai and H. Li, *J. Environ. Sci.*, **95**, 225 (2020); https://doi.org/10.1016/j.jes.2020.03.035
30. O.Y. Bakather, *Ain Shams Eng. J.*, **11**, 905 (2020); https://doi.org/10.1016/j.asej.2020.03.012
31. B. Heibati, K.J.G. Pollitt, A. Karimi, J. Yazdani Charati, A. Ducatman, M. Shokrzadeh and M. Mohammadyan, *Ecotoxicol. Environ. Saf.*, **144**, 445 (2017); https://doi.org/10.1016/j.ecoenv.2017.06.055
32. A. Mustafa, M.K. Azim, Z. Raza and J.A. Kori, *Chem. Eng. J.*, **333**, 451 (2018); https://doi.org/10.1016/j.cej.2017.09.168
33. B. Zhang, M. Chen, C. Zhang and H. He, *Chemosphere*, **217**, 780 (2019); https://doi.org/10.1016/j.chemosphere.2018.10.222
34. W.U. Rahman, M.D. Khan, M.Z. Khan and G. Halder, *J. Environ. Chem. Eng.*, **6**, 2957 (2018); https://doi.org/10.1016/j.jece.2018.04.038
35. N. Rahmani, A. Amiri, G.M. Ziarani and A. Badiei, *Mol. Catal.*, **515**, 111873 (2021); https://doi.org/10.1016/j.mcat.2021.111873
36. H. Hosseinzadeh asl, G. Tohidi, F. Movahedi and E. Hassannayebi, *J. Saudi Chem. Soc.*, **25**, 101371 (2021); https://doi.org/10.1016/j.jscs.2021.101371.
37. D. Yuan, X. Chen, Z. Li, C. Fang, J. Ding, H. Wan and G. Guan, *Appl. Surf. Sci.*, **569**, 151089 (2021); https://doi.org/10.1016/j.apsusc.2021.151089
38. C.-W. Lin, C.-H. Wu, P.-Y. Guo and S.-H. Chang, *J. Environ. Manage.*, **204**, 12 (2017); https://doi.org/10.1016/j.jenvman.2017.05.035
39. J.L. Gonzalez, A. Pell, L.-M. Montserrat and M. Valiente, *Sci. Total Environ.*, **603-604**, 109 (2017); https://doi.org/10.1016/j.scitotenv.2017.05.267
40. H.M. Giang, N.T. Huyen Nga, E.R. Rene, H.N. Ha and S. Varjani, *Environ. Res.*, **217**, 114788 (2023); https://doi.org/10.1016/j.envres.2022.114788

41. S. Kodama, S. Matsumoto, Y. Takamura, M. Fujihara, M. Watanabe, A. Ono and H. Kakuta, *Toxicol. Lett.*, **373**, 76 (2023); https://doi.org/10.1016/j.toxlet.2022.11.003
42. M. Li, W. Zhang, X. Zhang, Y. Lian, X. Niu and Y. Zhu, *J. Colloid Interface Sci.*, **630**, 301 (2023); https://doi.org/10.1016/j.jcis.2022.10.107
43. T. Wang, H. Zhang, K. Wang, M. Cao, M. Zhang, R. Sun, Y. Pu and J. Zhang, *Ecotoxicol. Environ. Saf.*, **226**, 112803 (2021); https://doi.org/10.1016/j.ecoenv.2021.112803
44. T. Kim, J. Lee, B. Lee, J. Park, S. Song, B.-K. Kim and S.Y. Kim, *Polymer*, **230**, 124105 (2021); https://doi.org/10.1016/j.polymer.2021.124105
45. A. Khan, J.E. Szulejko, P. Samaddar, K.-H. Kim, B. Liu, H.A. Maitlo, X. Yang and Y.S. Ok, *Chem. Eng. J.*, **361**, 1576 (2019); https://doi.org/10.1016/j.cej.2018.10.193
46. A. Šoštarić, S. Stanišić Stojić, G. Vuković, Z. Mijić, A. Stojić and I. Gržetić, *Atmos. Environ.*, **168**, 46 (2018); https://doi.org/10.1016/j.atmosenv.2017.08.045
47. I. Akmirza, C. Pascual, A. Carvajal, R. Pérez, R. Muñoz and R. Lebrero, *Sci. Total Environ.*, **587**, 457 (2018); https://doi.org/10.1016/j.scitotenv.2017.02.130
48. C.-F. Yang, S.-H. Liu, Y.-M. Su, Y.-R. Chen, C.-W. Lin and K.-L. Lin, *Sci. Total Environ.*, **648**, 811 (2019); https://doi.org/10.1016/j.scitotenv.2018.08.208
49. T. Han, J. Liu, M. Du, H. Xu, J. Dong, X. Li and H. Ge, *J. Fuel Chem. Technol.*, **49**, 1620 (2021); https://doi.org/10.1016/S1872-5813(21)60123-8
50. Y. Liu, W. Gao, J. Zhan, Y. Bao, R. Cao, H. Zhou and L. Liu, *Chem. Eng. J.*, **375**, 121956 (2019); https://doi.org/10.1016/j.cej.2019.121956
51. Z. Yang, J. Liu, X. Yao, Z. Rui and H. Ji, *Sep. Purif. Technol.*, **158**, 417 (2016); https://doi.org/10.1016/j.seppur.2015.12.027
52. Y. Wang, C. Yao, Y. Cao, C. Zhang and W. Tang, *Ceram. Int.*, **49**, 1137 (2023); https://doi.org/10.1016/j.ceramint.2022.09.090
53. A. Šoštarić, A. Stojić, S. Stanišić Stojić and I. Gržetić, *Chemosphere*, **144**, 721 (2016); https://doi.org/10.1016/j.chemosphere.2015.09.042
54. E.M. Elsehly, N.G. Chechenin, A.V. Makunin, D.A. Pankratov and H.A. Motaweh, *J. Water Process Eng.*, **25**, 81 (2018); https://doi.org/10.1016/j.jwpe.2018.06.005.
55. P.M. Stahelin, A. Valeria, M.D.A.G.U.D.S. Selene, A. Silva and A.B.V. Lose, *Fuel*, **231**, 45 (2018); https://doi.org/10.1016/j.fuel.2018.04.169
56. P.M. Stähelin, A. Valério, S.M.A. Guelli Ulson de Souza, A. da Silva, J.A. Borges Valle and A.A. Ulson de Souza, *J. Hazard. Mater.*, **326**, 229 (2017); https://doi.org/10.1016/j.jhazmat.2016.12.005
57. B.T. Mohammad, E.R. Rene, M.C. Veiga and C. Kennes, *Int. Biodeterior. Biodegradation*, **119**, 289 (2017); https://doi.org/10.1016/j.ibiod.2016.10.054
58. C.-W. Lin, C.-H. Wu, P.-Y. Guo and S.-H. Chang, *J. Environ. Manage.*, **204**, 12 (2017); https://doi.org/10.1016/j.jenvman.2017.05.035
59. R.C. Pepino Minetti, H.R. Macaño, J. Britch and M.C. Allende, *J. Hazard. Mater.*, **324**, 448 (2017); https://doi.org/10.1016/j.jhazmat.2016.11.010
60. A. Jaggi, R.W. Snowdon, A. Stopford, J.R. Radović, T.B.P. Oldenburg and S.R. Larter, *Org. Geochem.*, **108**, 1 (2017); https://doi.org/10.1016/j.orggeochem.2017.03.006.
61. A. Masih, A.S. Lall, A. Taneja and R. Singhvi, *Atmos. Environ.*, **147**, 55 (2016); https://doi.org/10.1016/j.atmosenv.2016.09.067
62. J. Li, G. Yan, L. Zhou, X. Bai and X. Chen, *Colloids Surf. A Physicochem. Eng. Asp.*, **657**, 130634 (2023); https://doi.org/10.1016/j.colsurfa.2022.130634
63. L. Wang, Q. Liu, C. Jing, J. Yin, N. Mominou and S. Li, *J. Hazard. Mater.*, **342**, 758 (2018); https://doi.org/10.1016/j.jhazmat.2017.09.003